



A new preload mechanism for a high-speed piezoelectric stack nanopositioner



Yuen Kuan Yong*

School of Electrical Engineering and Computer Science, The University of Newcastle, Callaghan, NSW 2308, Australia

ARTICLE INFO

Article history:

Received 17 September 2015

Revised 19 February 2016

Accepted 23 March 2016

Available online 12 April 2016

Keywords:

Preload

Piezoelectric stack actuator

Flexure

Nanopositioning

High-speed

ABSTRACT

Piezoelectric stack actuators are the actuator of choice for many ultra-high precision systems owing to its fast responses and high pushing force capabilities. These actuators are constructed by bonding multiple piezoelectric layers together. An inevitable drawback of these actuators is that there are highly intolerant to tensile and shear forces. During high-speed operations, inertial forces due to effective mass of the system cause the actuators to experience excessive tensile forces. To avoid damage to the actuators, preload must be applied to compensate for these forces. In many nanopositioning systems, flexures are used to provide preload to the piezoelectric stack actuators. However, for high-speed systems with stiff flexures, displacing the flexures and sliding the actuators in place to preload them is a difficult task. One may reduce the stiffness of the flexures to make the preload process more feasible; however, this reduces the mechanical bandwidth of the system. This paper presents a novel preload mechanism that tackles the limitations mentioned above. The preload stage, which is connected in parallel mechanically to a high-speed vertical nanopositioner, allows the piezoelectric stack actuator to be installed and preloaded easily without significantly trading of the stiffness and speed of the nanopositioning system. The proposed vertical nanopositioner has a travel range of 10.6 μm . Its first resonant mode appears at about 24 kHz along the actuation direction.

© 2016 Elsevier Ltd. All rights reserved.

1. Introduction

Piezoelectric stack actuators have been used in many high-speed nanopositioners [1–7] and precision systems [8–11] due to their high-bandwidth and large pushing force capabilities. The fundamental component of piezoelectric stack actuator is a thin layer of piezoelectric material sandwiched by two electrodes. All of these piezoelectric layers are poled in the direction of their thickness as illustrated in Fig. 1. The piezoelectric layers are bonded in series mechanically with opposite poling direction to each other. Their electrodes are connected in such a way that the layers are in parallel electrically. When a voltage V is applied to the piezoelectric stack actuator, its estimated total displacement is $\Delta l = nVd_{33}$, where n is the number of piezoelectric layers, and d_{33} is the piezoelectric coefficient. Without load, Δl is roughly around 0.1% to 0.15% of the actuator length [12].

Piezoelectric stack actuator is highly vulnerable to tensile and lateral forces [12]. High inertial force due to effective mass of the nanopositioning system during high-speed operations could potentially damage the actuator [13,14]. A common practice to avoid

such damage is to mechanically preload the actuator in the installation to compensate for these forces. A conventional preload mechanism involves a preload screw and block [1,15–17], as illustrated in Fig. 2(a). The screw is used to push the preload block against the piezoelectric stack actuator. Whilst this preload method is simple and effective for low-speed operations, at high-speed the screw and preload block act as a mass-spring system that interferes with the dynamics of the nanopositioning system. Another common way of preloading the actuator is to use a pair of wedges [16–19] as shown in Fig. 2(b). One of the wedges is attached to the actuator. When the other wedge is pushed down, the actuator is pushed forward due to the slope of the wedges. As a result, a preload is applied to the actuator. This preload method may induce lateral forces to the piezoelectric stack actuator which could potentially damage it. Some other preload methods include using permanent magnets [20], a preload bolt [21] and a dual-stack with bidirectional actuation [22].

Flexures have been used in many high-speed nanopositioner designs to simultaneously preload and guide the motion of the piezoelectric actuators [23–25]. To install and preload the actuators in these high-speed systems, forces are applied to elastically deform the flexures in order to make room for the actuators [see Fig. 2(c)]. The piezoelectric stack actuators are gently slid into

* Tel.: +61249216438.

E-mail address: yuenkuan.yong@newcastle.edu.au

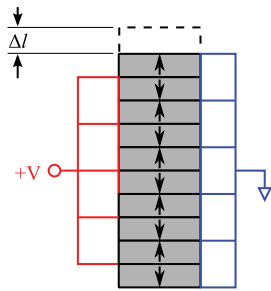


Fig. 1. Piezoelectric stack actuator.

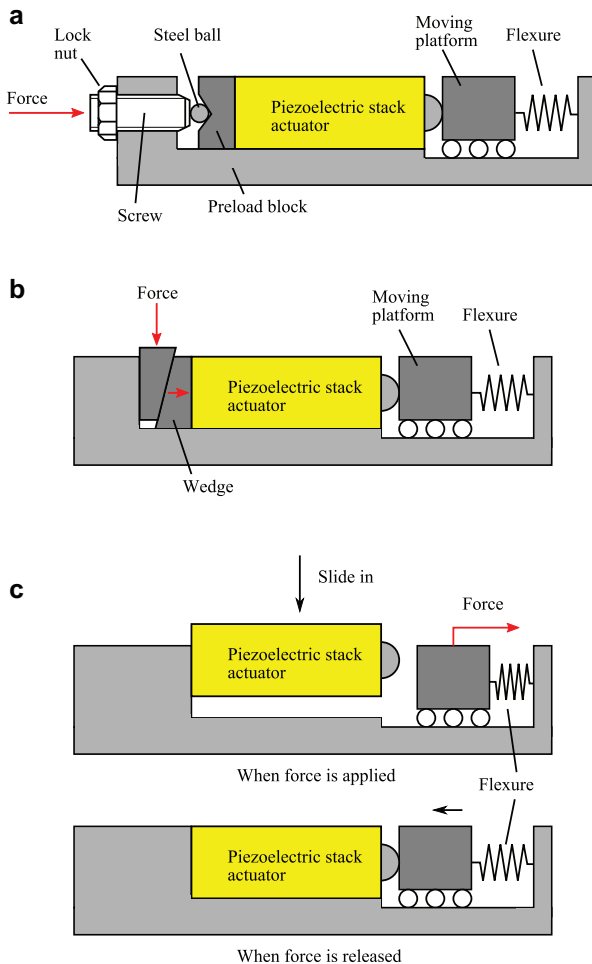


Fig. 2. Common preload methods.

their designated spaces. The applied forces are then released to restore the flexures to their original position in order to clamp the actuators in place. For high-speed systems, flexures are designed to be stiff (about 10% of the actuator's stiffness) in order to achieve high mechanical bandwidth [1]. Displacing these stiff flexures is a difficult task. For example, to deform a set of flexures with effective stiffness of $10 \text{ N}/\mu\text{m}$ [23,24] by 0.1 mm, a large pulling force of 1000 N is required. It is impractical to hang a 100 kg dead weight on the flexures to deform them. A carefully designed pulley system or a high-force preloading tool may be needed for this challenging task. Another approach to make the preload procedure more feasible is to reduce the stiffness of the flexures, however, this also reduces the resonances and speed of the nanopositioning system.

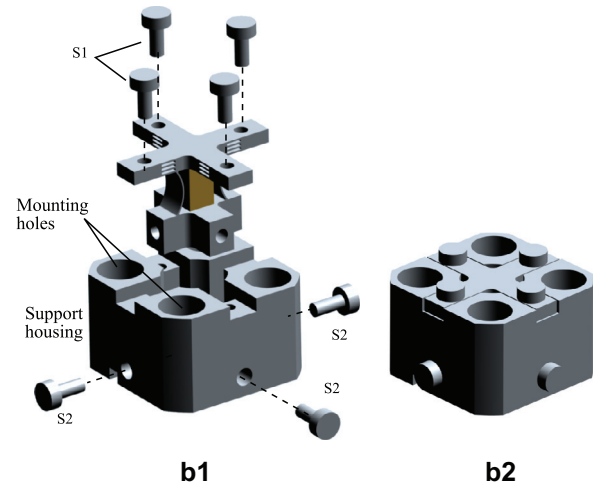
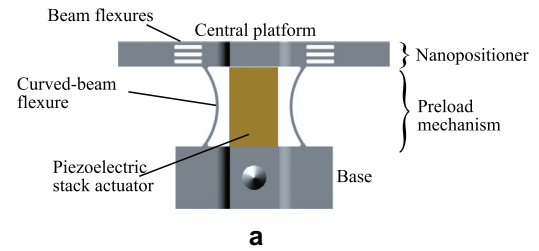


Fig. 3. (a) A high-speed vertical nanopositioner with a novel preload mechanism. (b1) An exploded view showing the nanopositioner and its support housing. (b2) Assembled view of the nanopositioning system.

This paper proposes a novel preload mechanism which deals with the aforementioned challenges in high-speed nanopositioning systems. The proposed nanopositioner design is a single-axis high-speed vertical stage. Vertical nanopositioning stages have many applications in the area of precision positioning, such as in the field of atomic force microscopy [5], alignment of optics [12,26], and objective scanners [27,28]. The preload stage, which is connected in parallel mechanically to a high-speed nanopositioner, allows for the ease of preloading and installation of the piezoelectric stack actuator without significantly trading-off the stiffness of the nanopositioning system.

The remainder of the paper is organized as follows. Section 2 describes the design configuration of the proposed nanopositioner. Stiffness and stress analysis of the nanopositioner is presented. Range and resonance frequency of the system are also estimated and presented in this section. Section 4 presents the experimental results of the nanopositioner. Conclusions are drawn in Section 5.

2. Design analysis of the nanopositioner

A high-speed vertical nanopositioner with a novel preload mechanism is shown in Fig. 3. The nanopositioning stage consists of four sets of beam-flexures to guide the motion of the central platform, and to provide the requisite stiffness to the structure. Mechanically in parallel is the preload mechanism that consists of two curved-beams. These curved-beams connect the central platform to the base of the device. A piezoelectric stack actuator is located between the platform and base. When a voltage is applied to the actuator, it displaces vertically, which in turn, elastically deforms the flexures to move the central platform vertically.

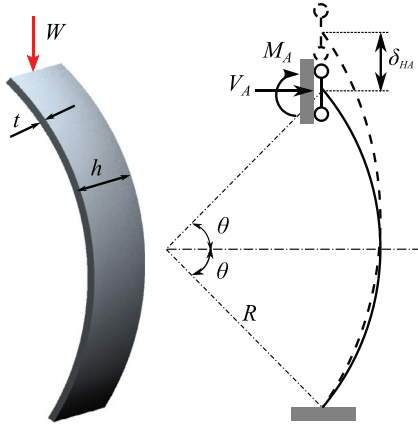


Fig. 4. Parameters of a fixed-guided curved-beam.

2.1. Preload mechanism design

The curved-beams of the preload mechanism were designed to be much compliance than that of the nanopositioner. This is to minimize the effect of the preload mechanism to the dynamics of the nanopositioner. During preloading, the central platform was fixed. A pulling force was applied to the base to displace the flexures, thus elongating the cavity in order to accommodate the piezoelectric stack actuator. After the actuator was placed, the pulling force was released. The curved-beams then return to its original position, and hence clamping the actuator into position.

2.1.1. Deformation and stiffness analysis

The amount of pulling force needed to elongate the curved-beams relies on their stiffness. For a fixed-guided curved-beam as shown in Fig. 4, its vertical stiffness can be estimated using Roark's formulations [29], that is

$$\delta_{HA} = \frac{R^3}{EI} \left(B_{HV} V_A + B_{HM} \frac{M_A}{R} - LF_H \right), \quad (1)$$

where R is the radius to the centroid of the cross-section; $I = t^3 h / 12$ is the area moment of inertia of the cross-section about the principal axis perpendicular to the plane of the curve; E is the Young's modulus; B_{HV} and B_{HM} are coefficients which can be estimated in Eq. (3). LF_H is a loading term given in Eq. (4). V_A and M_A are the reaction force and moment respectively at the guided-end of the beam as shown in Fig. 4, which are expressed as

$$\begin{aligned} V_A &= \frac{B_{MM} LF_V - B_{MV} LF_M}{B_{VV} B_{MM} - B_{MV}^2}, \\ \frac{M_A}{R} &= \frac{B_{VV} LF_M - B_{MV} LF_V}{B_{VV} B_{MM} - B_{MV}^2}, \end{aligned} \quad (2)$$

where

$$\begin{aligned} B_{MM} &= 2\theta, \\ B_{MV} &= 2\theta s, \\ B_{VV} &= 2\theta s^2 + k_1(\theta + sc) - k_2 2sc, \\ B_{HV} &= -2\theta sc + k_2 2s^2, \\ B_{HM} &= -2\theta c + k_2 2s. \end{aligned} \quad (3)$$

$s = \sin(\theta)$, $c = \cos(\theta)$, $n = \sin(\phi)$, and $m = \cos(\phi)$. θ is one-half of the total subtended angle of the curve. It is limited to the range zero to π . ϕ is the angle measured counterclockwise from the midspan of the curve to the position of the applied load W . In the case of the proposed curved-beam here, $\theta = \phi$. For the case of thin beams, k_1 and k_2 can be set to unity.

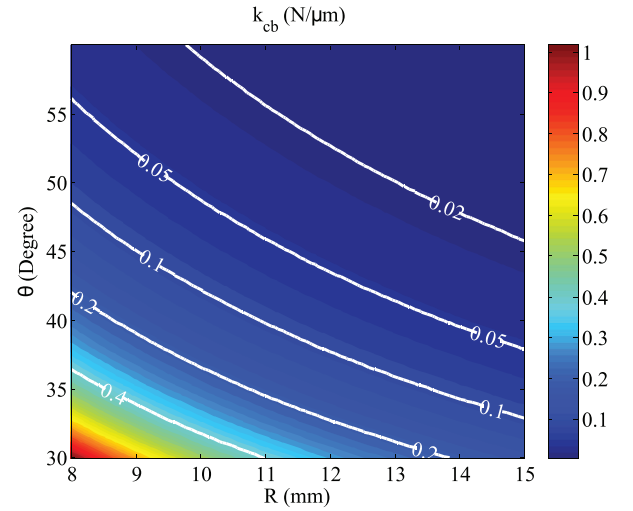


Fig. 5. Stiffness of the first mechanism plotted against θ and R .

For a fixed-guided boundary condition with a concentrated load W , the loading terms LF_H , LF_V and LF_M are [29]

$$\begin{aligned} LF_H &= W \left[(\theta + \phi) mc + \frac{k_1}{2} (\theta + \phi - sc - nm) \right. \\ &\quad \left. - k_2 (sm + cn) \right], \\ LF_V &= W \left[-(\theta + \phi) sm + \frac{k_1}{2} (c^2 - m^2) \right. \\ &\quad \left. + k_2 (1 - 2c^2 + cm + sn) \right], \\ LF_M &= W [-(\theta + \phi) m + k_2 (s + n)]. \end{aligned} \quad (4)$$

By substituting Eqs. (2)–(4) into (1), δ_{HA} can be expressed as a function of W . The stiffness of the curved-beam is therefore W/δ_{HA} . Since the two curved-beams are arranged in parallel, the stiffness of the preload mechanism, k_{cb} is

$$k_{cb} = \frac{2}{\delta_{HA}}. \quad (5)$$

A stiffness contour map is plotted against θ and R and is shown in Fig. 5. Note that t and h were selected to be 0.22 mm and 7 mm respectively. $t = 0.22$ mm is the smallest machinable thickness and $h = 7$ mm was chosen to be the same width as the piezoelectric stack actuator. Aluminum alloy 7075-T6 with $E = 72$ GPa, which is a common material used in flexure-based nanopositioner [1], was chosen.

2.1.2. Stress analysis

To ensure that the stack can be practically slid into the cavity without experiencing excessive lateral forces, it is a requisite to deform the curved-beams by at least $d = 0.35$ mm. In order to remain in the elastic region of the material, the following stress analysis is carried out to ensure that the curved-beams do not deform beyond the yield strength of the material. The maximum stress of the curved-beam is [29]

$$\sigma_i = \frac{k_i M c_h}{I}, \quad (6)$$

where

$$\begin{aligned} c_h &= \frac{t}{2}, \\ k_i &= \frac{1}{3e/c_h} \left(\frac{1 - e/c_h}{R/c_h - 1} \right), \\ \frac{e}{c_h} &= \frac{R}{c_h} - \frac{2}{\ln \frac{R/c_h + 1}{R/c_h - 1}}. \end{aligned} \quad (7)$$

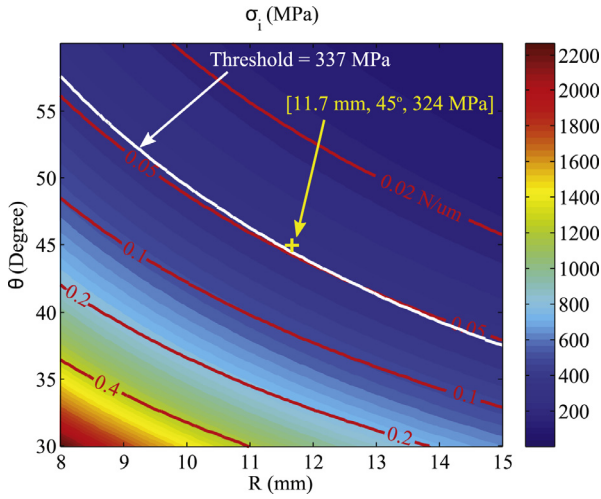


Fig. 6. A contour map of σ_i plotted against θ and R . The contour lines plotted in red are the stiffness of the curved-beams k_{cb} (For interpretation of the references to colour in this figure legend, the reader is referred to the web version of this article.).

The moment M is found using Eqs. (2)–(4) and $W = k_{cb}d/2$ (where $d = 0.35$ mm). According to the distortional energy density criterion (von-Mises) [30],

$$\sigma_i < \frac{S_y}{S_F}, \quad (8)$$

where S_y is the yield strength of the material, and $S_F = 1.5$ is the safety factor. A contour map of σ_i plotted against θ and R is shown in Fig. 6. The threshold limit $S_y/S_F = 337$ MPa is plotted in the figure. The stiffness contour, which is marked in red, is superimposed on the figure to assist with the design analysis.

The stiffness of the curved-beams should be soft enough to allow for the ease of deformation, and stiff enough so that it would not break easily while being handled. It should also be sufficiently stiff to provide the requisite preload to the actuator. The required preload is estimated from Newton's second law by calculating the maximum acceleration of the platform during maximum displacement and operating frequency. Assuming sinusoidal motion, the estimated dynamic (inertial) force on a piezoelectric stack actuator is [4,12]

$$F_i = 4\pi^2 M_{eff} \left(\frac{\Delta L}{2} \right) f^2, \quad (9)$$

where M_{eff} is the effective mass and ΔL is the maximum stroke. For example, to displace a 5 g mass at 5000 Hz over a $5 \mu\text{m}$ range, the minimum preload is approximately 12 N.¹ Given $k_{cb} = W/d$, and $d = 0.35$ mm, $W > 12$ N, k_{cb} should be at least 0.03 N/ μm . As a result, the properties of the curved-beams should satisfy the following requirements:

$$0.03 \text{ N}/\mu\text{m} \leq k_{cb} \leq 1 \text{ N}/\mu\text{m}, \quad (10)$$

$$\sigma_i \leq 337 \text{ MPa}.$$

Based on the above design criteria, $R = 11.7$ mm and $\theta = 45^\circ$ were chosen using Fig. 6. Their corresponding values σ_i and k_{cb} are 324 MPa and 0.046 N/ μm respectively. The R and θ values were chosen by taking into account of the compactness of the device. Summary of the final design values of the preload mechanism is exhibited in Table 1.

¹ Note that most nanopositioners are used to displace a smaller mass at much lower speeds. The 5-g mass at 5000 Hz are chosen here to ensure that extra preload is available to protect the stack during high-speed operations.

Table 1

Summary of material properties, design parameters and dimensions of flexures and piezoelectric stack actuators.

Aluminum alloy 7075-T6	Unit	Value
Young's modulus, E	GPa	72
Shear modulus, G	GPa	27
Poisson's ratio, ν		0.33
Yield strength, S_y	MPa	505
Piezoelectric stack actuator	Unit	Value
Young's modulus, E_a	GPa	52.6
Poisson's ratio, ν_a		0.32
Capacitance, C_a	nF	790
Stiffness, k_a	N/ μm	224.3
Nominal displacement, ΔL	μm	10.3
Curved-beam	Unit	Final design value
Thickness, t	mm	0.22
Depth, h	mm	7
Radius, R	mm	11.7
Subtended angle, θ	$^\circ$	45
Stage flexure	Unit	Final design value
Thickness, t_f	mm	0.45
Length, l_f	mm	3.3

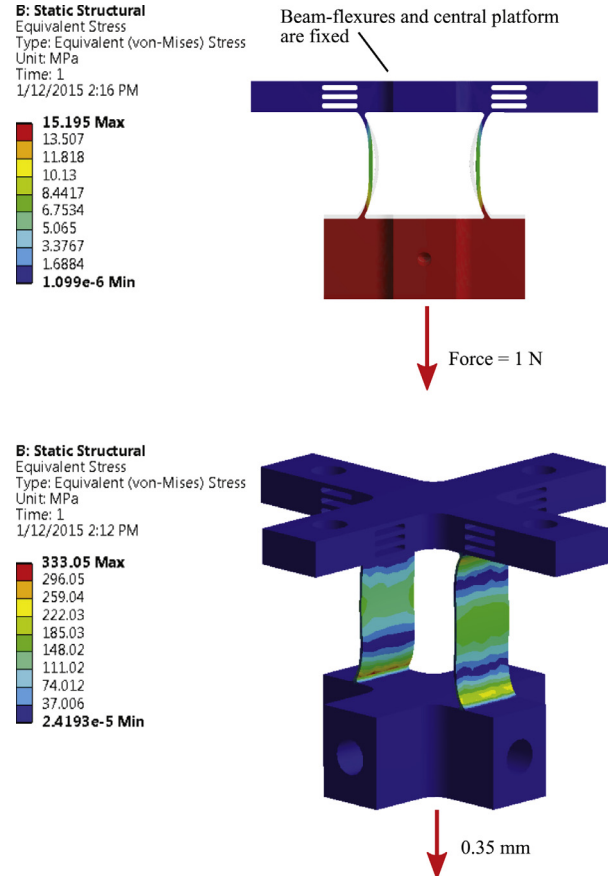


Fig. 7. Stiffness (top) and stress (bottom) estimations of the preload mechanism using ANSYS.

2.1.3. Finite-element-analysis

Stiffness and maximum equivalent stress (von-mises) of the curved-beams were investigated using a finite-element-analysis (FEA) package ANSYS. To simulate the stiffness, the beam-flexures and the central platform were fixed. Force was applied to the base as shown in Fig. 7. The deformation was then recorded to calculate

the stiffness. The simulated stiffness of the preload curved-beams is 0.066 N/ μ m. The maximum equivalent stress of the curved-beams was obtained using the similar boundary conditions, except that the force was replaced by a displacement of 0.35 mm. Fig. 7 shows that the maximum equivalent stress is 333 MPa.

The small discrepancy between the analytical and FEA results is due to the fact that the filleted corners of the curved beams were omitted in the analytical formulations. These filleted corners slightly increase the stiffness and maximum stress of the curved-beams. Nevertheless, the simulated stiffness and maximum equivalent stress satisfy the design criteria in Eq. (10).

2.2. High-speed nanopositioner design

The high-speed nanopositioning stage is guided by four sets of flexures. Each set consists of four beam-flexures. In order to design a high-speed nanopositioner with relatively large displacement (approximately 10 μ m), a custom made 7 mm \times 7 mm \times 11.5 mm piezoelectric stack actuator with a high stiffness, large force and large stroke is used. Two 2.6 mm alumina end plates are glued to each end of the piezoelectric stack actuator to extend its length in order to fit into the cavity of the nanopositioner. The actuator's properties can be found in Table 1.

2.2.1. Estimation of stiffness, range and resonance frequency

The stiffness of the nanopositioner k_s was designed to be approximately 10% of the stack for high-speed applications [1]. This amounts to approximately 20 N/ μ m. Details on how to design flexures for high-speed nanopositioning systems can be found in [1,4,23,24]. The chosen length l_f and thickness t_f of the beam-flexures are 3.3 mm and 0.45 mm respectively. The estimated stiffness k_s , travel range D_s and resonance frequency f_z can be calculated as follows [1,23,24]:

$$k_s = 16 \left[\frac{l_f^3}{Eht_f^3} + \frac{\alpha l_f}{Ght_f} \right]^{-1}, \quad (11)$$

$$D_s = \Delta L \frac{k_a}{k_s + k_a + k_{cb}}, \quad (12)$$

$$f_z = \frac{1}{2\pi} \sqrt{\frac{K_{eff}}{M_{eff}}}, \quad (13)$$

where K_{eff} and M_{eff} are the effective stiffness and mass of the system. Descriptions of the design parameters and their corresponding values can be found in Table 1. The estimated k_s , D_s and f_z are 19.3 N/ μ m, 9.5 μ m and 22.3 kHz respectively.

2.2.2. Finite-element-analysis

FEA was conducted to study the stiffness and resonance frequency of the nanopositioning system. To simulate the stiffness of the system, the base and the top four mounting holes were fixed as shown in Fig. 8. Force was applied to the center of the platform and the deformation was recorded. The simulated stiffness is calculated to be 21.7 N/ μ m which is in close agreement with that of the analytical result.

Resonance frequency of the system was simulated by modeling the entire assembled system which includes the nanopositioner, piezoelectric stack actuator and the support housing (see Fig. 3). The nanopositioner was secured to the housing and the four mounting holes on the support housing were fixed. The obtained first resonant mode was the actuation mode at 23.1 kHz, which is again in close agreement to the analytical result. Fig. 9 shows the first four resonant modes obtained using ANSYS. During high-speed operations, both in- and out-of-plane modes can be excited, and hence limiting the bandwidth and speed of the nanopositioning system. This vertical nanopositioner was designed in such

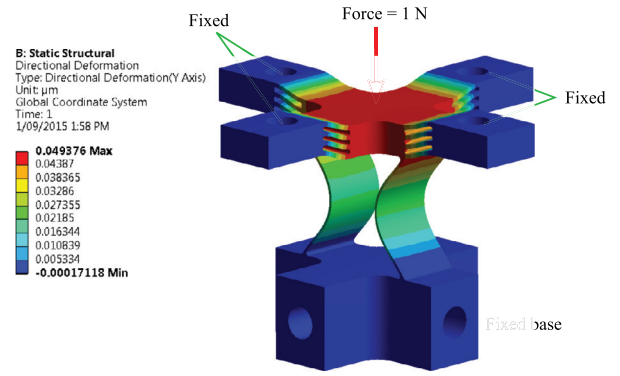


Fig. 8. Stiffness estimation of the nanopositioner using ANSYS.

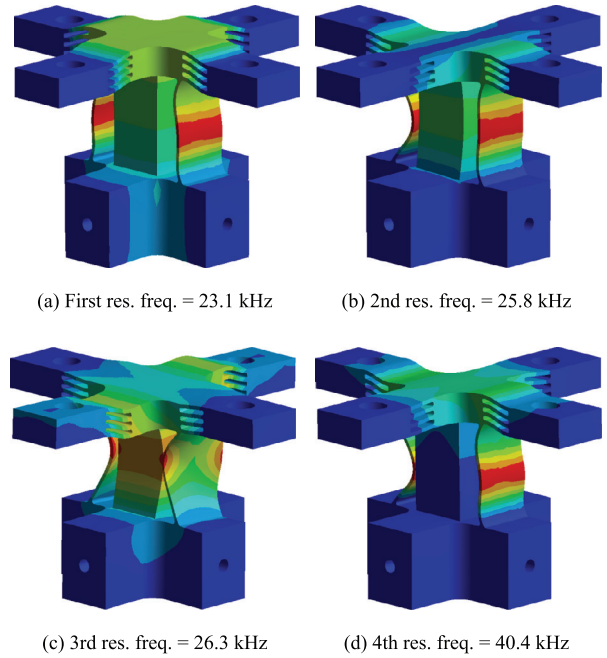


Fig. 9. Finite-element simulated resonance frequencies of the nanopositioner. Note that the support housing of the device was hidden in order to show the piezoelectric stack actuator and flexures.

a way that its actuation mode precedes the bending and other out-of-plane modes. This is desirable because the actuation mode is relatively straightforward to measure. Feedback control techniques can be implemented to effectively suppress the actuation mode in order to further increase the bandwidth [1,4,24]. This can not be achieved if other undesirable resonant modes precede the actuation mode.

3. Preloading piezoelectric stack actuator

Fig. 10 shows the setup for preloading the piezoelectric stack actuator. The central platform of the nanopositioner was fixed on a stationary front jig. A lock nut was secured onto the base of the nanopositioner. A fine pitch screw, which was held on a stationary back jig, was screwed onto the lock nut. When the screw was tightened, a pulling force was applied to the base and the curved-beams were deformed. The gap as shown in Fig. 10 was kept to approximately 0.35 mm using a filler gage. The piezoelectric stack actuator was slid in between the curved-beams. The screw was then loosened and the actuator was clamped into position. Note that a safety factor of 1.5 was used in the stress analysis in Section. 2.1.2. The gap can be set from 0.35 mm–0.5 mm. The

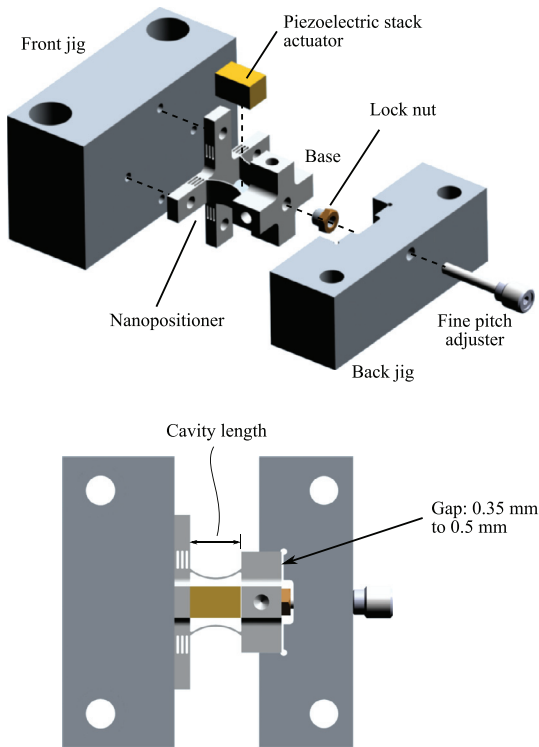


Fig. 10. Preload setup of the piezoelectric stack actuator.

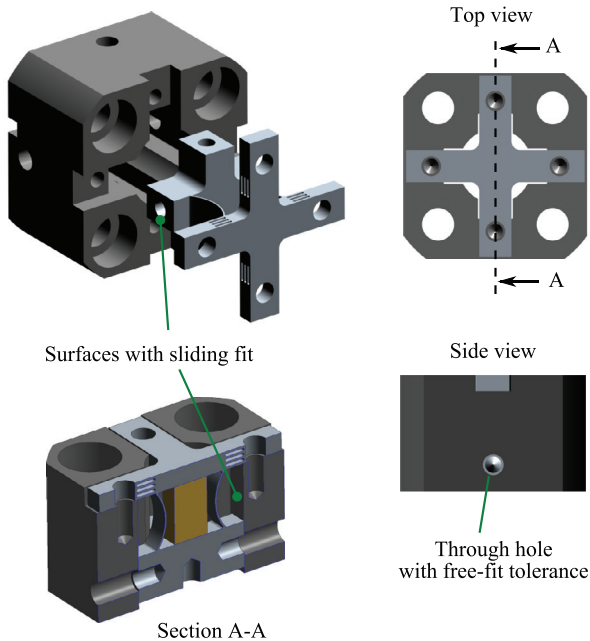


Fig. 11. Machining tolerances.

deformation of the curved-beam flexures within this range will remain in its elastic region.

3.1. Tolerances

The cavity length between the two curved-beam is 16.55 mm, which is 0.35 mm less than that of the piezoelectric stack actuator. It was machined with precision, with a tolerance of $+0.00/-0.02$ mm. The actuator length is ± 0.05 mm of its nominal value. Due to manufacturing errors and tolerances, the preload can vary

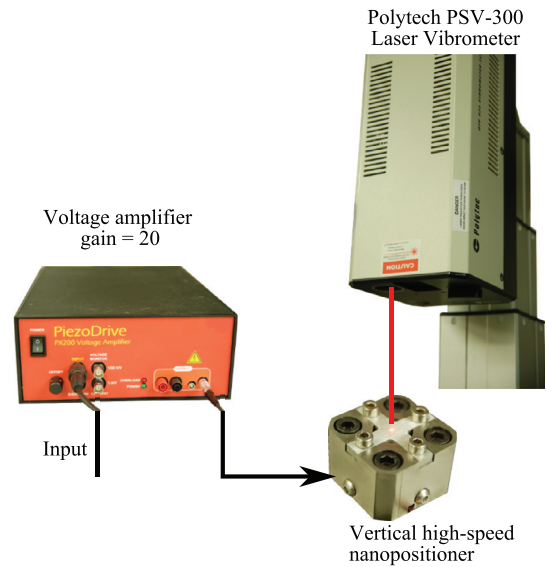


Fig. 12. Experimental setup of measuring the frequency response and travel range of the nanopositioner.

between 13.8 N–19.3 N. Nevertheless, this preload range is sufficient for moving a 5 g mass at 5 kHz as discussed in Section 2.1.2.

After piezoelectric stack actuator was installed, the nanopositioner was mounted to the support housing. The top four screws (S1) were secured first, followed by the bottom horizontal screws (S2) as shown in Fig. 3. Note that the contact surfaces between the base and support housing were machined with sliding fit precision as shown in Fig. 11. This is to avoid rotational motions of the base as well as to minimize unequal horizontal forces induced by the horizontal screws at the bottom of the housing during installation. The through holes on the support housing were machined with free fit tolerance, that is, in this case a 4.8 mm diameter hole for a M4 screw. This tolerance is sufficient to accommodate for machining errors. Furthermore, these holes are also offset by 0.35 mm to account for the additional distance after preloading the actuator.

It is worth mentioned here that the existing preload techniques in literatures involve using stiff flexures [23,24]. The combined stiffness of these flexures are approximately $10 \text{ N}/\mu\text{m}$ – $20 \text{ N}/\mu\text{m}$. To elongate the cavity by 0.35 mm for the installation of the piezoelectric stack actuator, a 3500 N–7000 N force is required which is impractical. The proposed curved-beam preload mechanism requires no more than 20 N. This can easily be achieved using a simple setup as shown in Fig. 10. The curved-beam mechanism provides sufficient preload to the actuator for high-speed operations and allows for ease of installation of actuator.

4. Experimental result

This section evaluates the dynamic performances of the high-speed nanopositioner. A Polytec PSV-300 laser scanning vibrometer was used to measure its displacement and resonance frequency as shown in Fig. 12. A high-bandwidth PX200 voltage amplifier from PiezoDrive, which has a gain of 20, was used to drive the piezoelectric stack actuator.

A small pseudo-random input signal with a bandwidth of 10 Hz–200 kHz was applied to the piezoelectric actuator to measure the resonance frequency of the nanopositioner. The measured frequency response is plotted in Fig. 13, showing its first resonant mode of 24 kHz. Note that there are no resonances appear before 24 kHz in the measured frequency response. This indicates that the dynamics of the preload mechanism does not degrade the high-speed performances of the nanopositioning system.

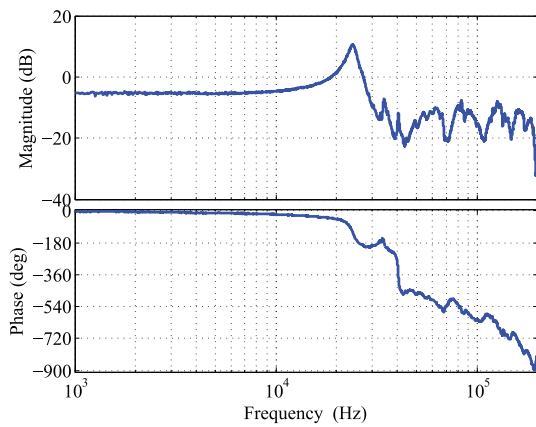


Fig. 13. Measured frequency response of the nanopositioner. The first resonant mode appears at 24 kHz.

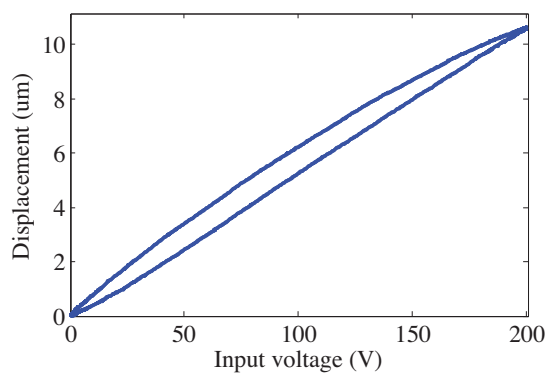


Fig. 14. Measured displacement range of the nanopositioner. The full-range of the nanopositioner is $10.6 \mu\text{m}$.

A 200 V peak-to-peak sinusoidal input at 100 Hz was applied to the actuator, and the displacement of the vertical nanopositioner was measured. The measured full-range displacement is $10.6 \mu\text{m}$. Fig. 14 illustrates the hysteresis profile of the nanopositioner. The width of the hysteresis loop is approximately $0.79 \mu\text{m}$, that is 9% of the full-range displacement of the nanopositioner.

Mode shapes of the central platform was also measured using the laser vibrometer. Fig. 15 shows the first three mode shapes of the system. They appear at 24 kHz, 66.5 kHz and 84.7 kHz respectively. All of these mode shapes are along the actuation direction, which are the preferred mode shapes from the control perspective.

5. Conclusions

A novel preload mechanism for a high-speed vertical nanopositioner was presented. The preload mechanism consists of two curved-beams which can be elastically deformed to accommodate and preload the piezoelectric stack actuator without significantly reducing the stiffness and speed of the nanopositioning system. The preload mechanism was also designed in such a way that it does not affect the dynamics of the nanopositioner. Experiments were conducted to evaluate the dynamic performances and travel range of the nanopositioner. The proposed high-speed nanopositioner has a first resonant mode at 24 kHz along the preferred actuation direction. Its measured travel range is $10.6 \mu\text{m}$. Feedback or feedforward control will be implemented to this preloaded high-speed nanopositioner in the near future for precision applications such as atomic force microscopy and alignment of optical systems.

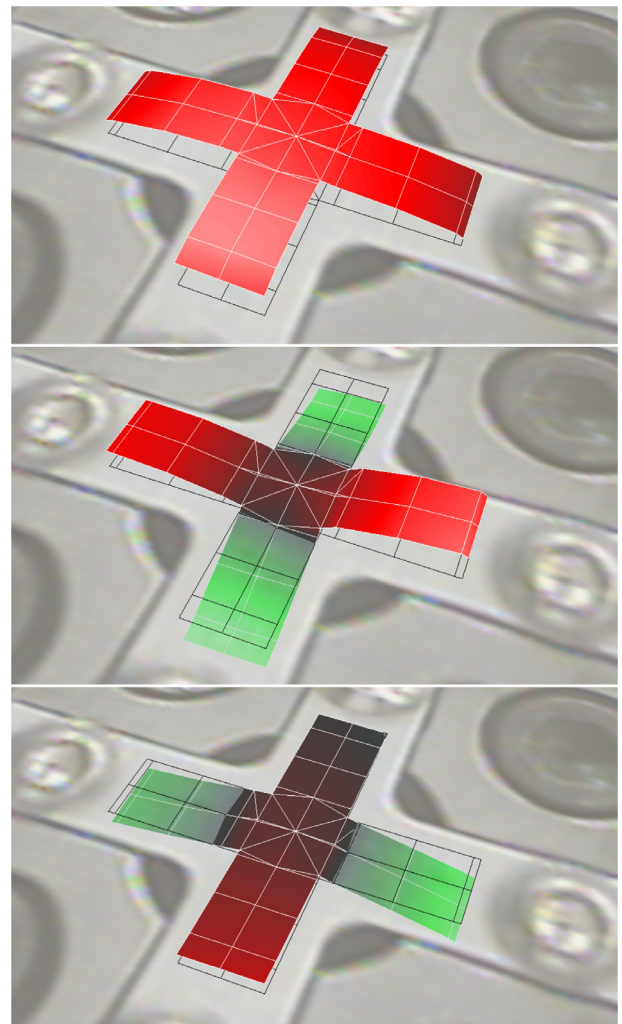


Fig. 15. Experimentally determined mode shapes of the nanopositioner. (Top) First mode: 24 kHz. (Middle) Second mode: 66.5 kHz. (Bottom) Third mode: 84.7 kHz. All three modes are the actuation mode along the vertical axis.

Acknowledgments

This work was supported by the Australian Research Council DECRA Project (DE130100879).

References

- [1] Yong YK, Moheimani SOR, Kenton BJ, Leang KK. Invited review article: high-speed flexure-guided nanopositioning: mechanical design and control issues. *Rev Sci Instrum* 2012;83(12):121101.
- [2] Wadikhaye S, Yong YK, Moheimani SOR. Design of a compact serial-kinematic scanner for high-speed atomic force microscopy: an analytical approach. *Micro Nano Lett* 2012;7(4):309–13.
- [3] Yong YK, Moheimani SOR. Design of an inertially counterbalanced Z-nanopositioner for high-speed atomic force microscopy. *IEEE/ASME Trans Nanotechnol* 2013;12(2):137–45.
- [4] Fleming AJ, Leang KK. Design, modeling and control of nanopositioning systems. London, UK: Springer; 2014. ISBN 978-3319066165.
- [5] Kenton BJ, Fleming AJ, Leang KK. Compact ultra-fast vertical nanopositioner for improving scanning probe microscope scan speed. *Rev Sci Instrum* 2011;82(12):123703.
- [6] Ando T. High-speed atomic force microscopy coming of age. *Nanotechnology* 2012;23(6):062001.
- [7] Schitter G, Åstrom KJ, DeMartini B, Thurner PJ, Turner KL, Hansma PK. Design and modeling of a high-speed AFM-scanner. *IEEE Trans Control Syst Technol* 2007;15(5):906–15.
- [8] Xu Q. Design and development of a flexure-based dual-stage nanopositioning system with minimum interference behavior. *IEEE Trans Autom Sci Eng* 2012;9(3):554–63. doi:10.1109/TASE.2012.2198918.

- [9] Li Y, Xu Q. Design and analysis of a totally decoupled flexure-based XY parallel micromanipulator. *IEEE Trans Robot* 2009;25(3):645–57.
- [10] Kim HS, Cho YM. Design and modeling of a novel 3-dof precision micro-stage. *Mechatronics* 2009;19(5):598–608.
- [11] Zheng J, Salton A, Fu M. Design and control of a rotary dual-stage actuator positioning system. *Mechatronics* 2011;21(6):1003–12.
- [12] Properties of piezo actuators. Physik Instrumente, Karlsruhe, Germany. <http://www.piezo.com/piezo-technology.html>.
- [13] Koruza J, Franzbach DJ, Schader F, Rojas V, Webber KG. Enhancing the operational range of piezoelectric actuators by uniaxial compressive preloading. *J Phys D: Appl Phys* 2015;48(21):215302.
- [14] Chaplya PM, Mitrovic M, Carman GP, Straub FK. Durability properties of piezoelectric stack actuators under combined electromechanical loading. *Journal of Applied Physics* 2006;100(12):124111. doi:10.1063/1.2407269.
- [15] Yong YK, Aphale S, Moheimani SOR. Design, identification and control of a flexure-based XY stage for fast nanoscale positioning. *IEEE Trans Nanotechnol* 2009;8(1):46–54.
- [16] Lu T-F, Handley DC, Yong YK, Eales C. A three-DOF compliant micromotion stage with flexure hinges. *Ind. Robot* 2004;31(4):355–61.
- [17] Wang R, Zhang X. Preload characteristics identification of the piezoelectric-actuated 1-DOF compliant nanopositioning platform. *Front Mech Eng* 2015;10(1):20–36. doi:10.1007/s11465-015-0328-z.
- [18] See Cedrat Technologies. <http://www.cedrat-technologies.com/>.
- [19] Handley D, Lu T-F, Yong Y, Zhang W. A simple and efficient dynamic modelling method for compliant micropositioning mechanisms using flexure hinges. In: Proceedings of SPIE on device and process technologies for MEMS, microelectronics, and photonics III, 5276; 2004. p. 67–76. doi:10.1117/12.523573.
- [20] Baek S, Han C, Lee C, Noh M. Design of a preload device for PZT actuator using permanent magnets. *IEEE Trans Magn* 2003;39(5):2965–7. doi:10.1109/TMAG.2003.816708.
- [21] DeAngelis DA, Schulze GW, Wong KS. Optimizing piezoelectric stack preload bolts in ultrasonic transducers. *Phys Procedia* 2015;63:11–20. doi:10.1016/j.phpro.2015.03.003.
- [22] Heverly DE, Wang KW, Smith EC. Dual-stack piezoelectric device with bidirectional actuation and improved performance. *J Intell Mater Syst Struct* 2004;15(7):565–74. doi:10.1177/1045389X04044450.
- [23] Kenton BJ, Leang KK. Design and control of a three-axis serial-kinematic high-bandwidth nanopositioner. *IEEE/ASME Trans Mechatronics* 2012;17(2):356–68.
- [24] Yong YK, Bhikkaji B, Moheimani SOR. Design, modeling and FPAA-based control of a high-speed atomic force microscope nanopositioner. *IEEE/ASME Trans Mechatronics* 2013;18(3):1060–71.
- [25] Wadikhaye S, Yong YK, Moheimani SOR, Bhikkaji B. Control of a piezoelectrically actuated high-speed serial kinematic AFM nanopositioner. *Smart Mater Struct* 2014;22(2) 025030(12pp).
- [26] See Mad City Labs Inc., <http://www.madcitylabs.com/> for information on flexure-based nanopositioning applications.
- [27] See Queensgate Instruments, <http://www.nanopositioning.com/> for information on flexure-based nanopositioning applications.
- [28] Hoffmann H. Nanopositioning in optics and photonics. Tech. Rep. Physik Instrumente GmbH & Co.; 2006.
- [29] Roark RJ, Young WC, Budynas RG. Roark's formulas for stress and strain. 7th ed. New York: McGraw-Hill; 2002. ISBN 0-07-072542-X.
- [30] Boresi AP, Schmidt RJ. Advanced mechanics of materials. 6th ed. Hoboken, New Jersey: John Wiley & Sons, Inc.; 2003.